Molecular Catalysis 515 (2021) 111926

Contents lists available at ScienceDirect

Molecular Catalysis

journal homepage: www.journals.elsevier.com/molecular-catalysis

CO oxidative coupling to dimethyl oxalate over Pd monolayer supported on SiC substrate: insight into the effects of different exposed terminals

Bingying Han [a], Mengjie Dong [a], Riguang Zhang [a], Lixia Ling [b,c,d,**], Maohong Fan [c], Ping Liu [d], Baojun Wang [a,*]

[a] State Key Laboratory of Clean and Efficient Coal Utilization, Taiyuan University of Technology, No. 79 West Yingze Street, Taiyuan 030024, PR China
[b] College of Chemistry and Chemical Engineering, Taiyuan University of Technology, Taiyuan 030024, PR China
[c] Department of Chemical and Petroleum Engineering, University of Wyoming, 1000 E University Ave, Laramie WY 82071, United States
[d] State Key Laboratory of Coal Conversion, Institute of Coal Chemistry, Chinese Academy of Sciences, Taiyuan 030001, PR China

ARTICLE INFO

Keywords:
Pd-based catalysts
Dimethyl oxalate
DFT
Micro-reaction kinetic model
Catalytic performance

ABSTRACT

Developing supported Pd-based catalysts with the low Pd amount and excellent catalytic performance is essential for CO oxidative coupling to dimethyl oxalate (DMO), where elucidating the effects of different exposed terminals of substrate materials on catalytic performance is crucial to the design of supported catalysts. Herein, Pd monolayer was supported on SiC with different exposed terminals, constructing the models of Pd_{ML}/SiC(111)-Si and Pd_{ML}/SiC(111)-C terminal, which was used to investigate the effects of different exposed terminals of substrate materials on DMO synthesis from CO and OCH_3. The density functional theory (DFT) calculations illustrated there existed no difference in the optimum path to generate DMO, which was $COOCH_3$-$COOCH_3$ coupling path on two catalysts. However, the rate control steps of the optimum path were different, with $2COOCH_3 \rightarrow$ DMO on the Pd_{ML}/SiC(111)-Si terminal and $COOCH_3 + (CO + OCH_3) \rightarrow 2COOCH_3$ on the Pd_{ML}/SiC (111)-C terminal. The micro-reaction kinetic model analysis further showed that the catalytic performance of Pd_{ML}/SiC(111)-Si terminal was favorable than that of Pd_{ML}/SiC(111)-C terminal, mainly attributing to that the difference in the exposed terminals of substrate materials led to the different electrons transfer directions of the Pd monolayer, then changed the adsorption energy of reactants (CO, OCH_3) and key intermediates ($COOCH_3$, $OCCOOCH_3$), and further changed rate control step of the optimum path. This work offers the insights in rational design of supported Pd-based catalyst for heterogeneous catalytic reaction.

1. Introduction

Coal resources into high value-added chemical products have attracted widespread research interest of scientists, because it can not only reduce the pollution caused by coal burning but also increase the economic added value of coal resources [1–7]. Specially, the coal-to-ethylene glycol (CTEG) as a green clean and high efficient production process in C1 chemistry field, is growing on more prosperously [8–12]. The CO oxidative coupling to DMO is known as the most essential procedure in CTEG process [13–15]. In addition to the main product DMO, the by-product dimethyl carbonate (DMC) is also be formed in the procedure of CO oxidative coupling to DMO. It has been confirmed that Pd-based catalysts exhibited the best activity and selectivity for catalyzing CO oxidation to DMO [16]. However, the expensive price and high dosage of Pd increase production costs [17]. Hence, developing supported Pd-based catalysts with the low Pd usage and excellent catalytic performance is imperative for this process.

Silicon carbide (SiC) as an excellent substrate owing to its outstanding properties of high mechanical strength, thermal conductivity, and oxidation resistance, was widely employed in heterogeneous catalytic reaction [18–21]. Guo et al. [22] adopted SiC material as substrate to prepare Pd/SiC catalyst through the incipient wetness impregnation method, and found that the high thermal conductivity of SiC support facilitated the fast temperature homogenization of the catalyst bed, which induced that Pd/SiC catalyst possessed a stable and excellent catalytic performance for hydrogenation reaction of acetylene. It was also found that Pd/SiC catalyst showed very high catalytic activity and stability in the catalytic combustion of low concentration methane

** Corresponding author at: College of Chemistry and Chemical Engineering, Taiyuan University of Technology, Taiyuan 030024, PR China.
* Corresponding author.
E-mail addresses: linglixia@tyut.edu.cn (L. Ling), wangbaojun@tyut.edu.cn (B. Wang).

https://doi.org/10.1016/j.mcat.2021.111926

Available online 9 October 2021

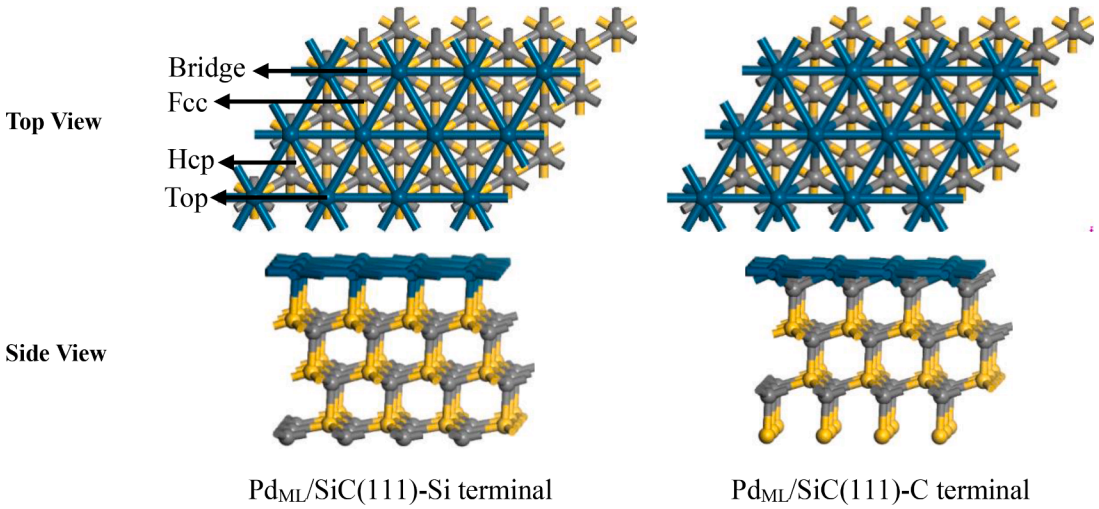

Fig. 1. The structure of Pd_{ML}/SiC(111)-Si and Pd_{ML}/SiC(111)-C terminal as well as the corresponding possible adsorption sites. (Dark cyan ball, Pd; yellow ball, Si; gray ball, C) (For interpretation of the references to color in this figure legend, the reader is referred to the web version of this article.).

[23]. Pd was deposited on the surface of irregular SiC, which was used to study the bonding between Pd and SiC. The results showed that Pd and irregular SiC not only formed Pd-Si bond, but also formed Pd-C bond [24]. The adsorption properties of small molecules, such as pyrrole, has been studied on the SiC-Si terminal and SiC-—C terminal [25]. It was shown that the adsorption energy of pyrrole was different on different exposed terminal of SiC.

As well known, the catalytic performance has a strong correlation with the adsorption energy of small molecules on catalysts [26,27]. For example, for the DMO synthesis from CO and OCH_3, previous study testified the moderately strong CO chemisorption energy on Pd-based catalyst was beneficial for the activation of CO and the formation of DMO [28]. The differences in adsorption energies would lead to differences in the energy barriers of the elementary reaction, resulting in different catalytic performance.

Nowadays, fundamental theoretical studies with density function theory (DFT) computations [29–33] have provided significant insights into the reaction mechanism and structural-performance relationship for catalytic reaction system. The micro-reaction kinetic model [34-38] is the link between the micro and practical reaction, which is used to calculate the formation rate of product under actual reaction conditions. In the work, the DFT computations combined with the micro-reaction kinetic model analysis have been adopted to study DMO synthesis from CO and OCH_3 on Pd_{ML}/SiC(111)-Si and Pd_{ML}/SiC(111)-C terminal which represent SiC with different exposed terminals supporting Pd monolayer, so as to elucidate the effects of different exposed terminals on catalytic performance and obtain excellent catalytic performance of SiC supporting Pd monolayer catalyst.

2. Computational methods and models

The Vienna ab-initio simulation package (VASP) has been utilized to fulfill all the DFT calculations in this work [39,40]. The Perdew-Burke-Ernzerh (PBE) function about Generalized Gradient Approximation (GGA) [41] was utilized to describe the exchange-correlation energies. The Projector-Augmented Wave (PAW) function [42,43] was utilized to depict the interaction between electron and ion. The cutoff energy about plane wave basis was set within the 400 eV. The Brillouin zone was sampled in setting the (3 × 2 × 1) of k-point mesh. The electronic energies of self-successive iteration was converged within 1×10^{-5} eV, meantime the convergence of the force change on each atom must be low than 0.03 eV•$Å^{-1}$. The transition state (TS) structure was searched via adopting the Climbing-Image Nudged Elastic Band (CI-NEB) [44,45] united dimer approach [46,47]. The forces change on each atom for the optimized transition state structure was below 0.05 eV•$Å^{-1}$. When there existed a sole imaginary frequency along the reaction coordinate, the transition state structure was considered to be reasonable.

The SiC(111)-Si and SiC(111)-C terminal were modeled firstly via constructing a seven-atom layers with the supercell size of (3 × 4), respectively. Then, the atoms on the surface layer of SiC(111)-Si and SiC (111)-C terminal were replaced with Pd atoms, i.e. Pd_{ML}/SiC(111)-C and Pd_{ML}/SiC(111)-Si terminal, as depicted in Fig. 1. The 15 Å vacuum was set to guard against the repeated slabs interaction. In order to reflect the bulk properties of the Pd_{ML}/SiC(111)-Si and Pd_{ML}/SiC(111)-C terminal in the practical reaction, the bottom two layers were set to be fixed, while the topmost five layers together with the adsorbed species were set to be relaxed.

In this work, all the electronic energy was rectified by the zero-point energy (ZPE) which was calculated via the following formula (1). Here, h and ν_i referred to Planck constant and real frequency, respectively.

$$\mathrm{ZPE} = \sum_{i=1} \frac{hvi}{2} \tag{1}$$

The adsorption energy (E_{ads}) was calculated by the following formula (2). $E_{slab/adsorbate}$ was the total energy of the slab together with adsorbate; E_{slab} and $E_{adsorbate}$ were energy of slab and isolated adsorbate, respectively.

$$E_{ads} = E_{slab/adsorbate} - E_{slab} - E_{adsorbate} \tag{2}$$

The reaction energy (ΔE_f) and activation energy ($E_{a,f}$) of forward reaction as well as the reaction energy (ΔE_r) and activation energy ($E_{a,r}$) of reverse reaction were obtained via the following formulas (3), (4), (5) and (6). E_{FS}, E_{IS}, E_{TS} were the energy of final, initial, and transition state, respectively.

$$\Delta E_f = E_{FS} - E_{IS} \tag{3}$$

$$E_{a,f} = E_{TS} - E_{IS} \tag{4}$$

$$\Delta E_r = E_{IS} - E_{FS} \tag{5}$$

$$E_{a,r} = E_{TS} - E_{FS} \tag{6}$$

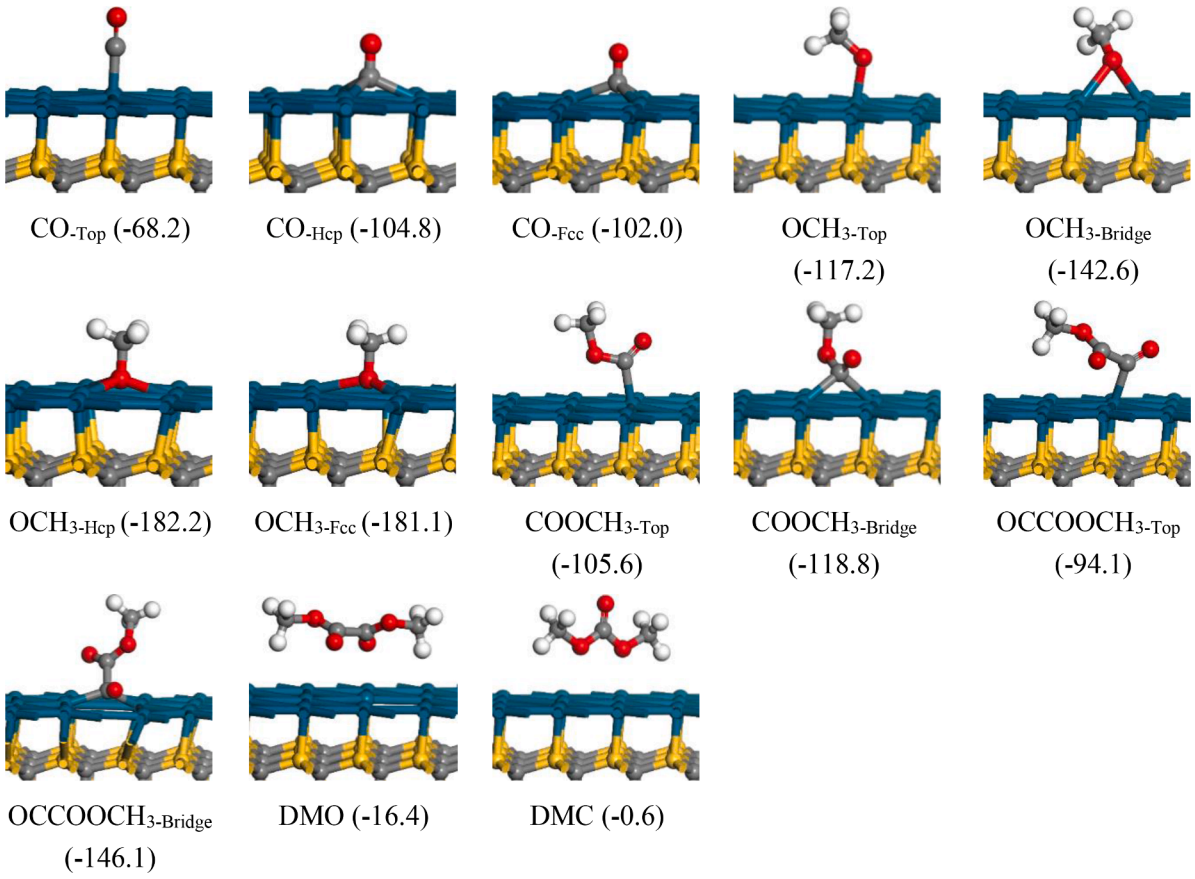

Fig. 2. Possible adsorption configurations of all species on the Pd_{ML}/SiC(111)-Si terminal and the corrected adsorption energies (kJ•mol^{-1}) by the zero-point energy (ZPE).

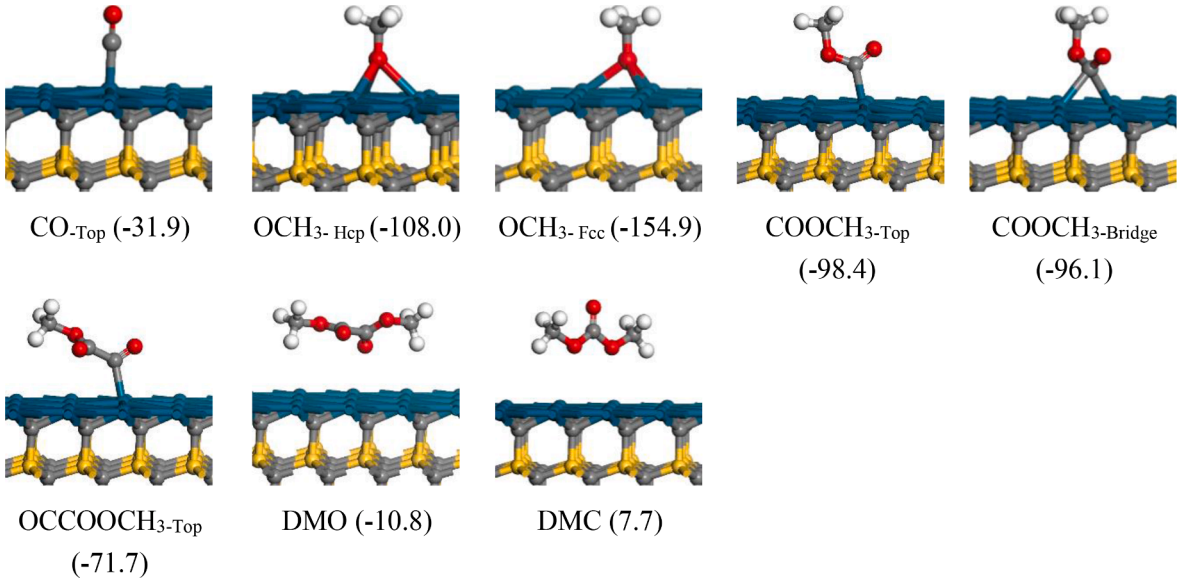

Fig. 3. Possible adsorption configurations of all species on the Pd_{ML}/SiC(111)-C terminal and the corrected adsorption energies (kJ•mol^{-1}) by the zero-point energy (ZPE).

3. Results and discussion

3.1. Possible adsorption of all species

The possible adsorption configurations of all species involved in CO oxidative coupling to DMO and the corrected adsorption energies by the zero-point energy (ZPE) have been calculated over Pd_{ML}/SiC(111)-Si and Pd_{ML}/SiC(111)-C terminal. The results were depicted in Figs. 2 and 3, and the detailed discussion was described as follows.

On the Pd_{ML}/SiC(111)-Si terminal, the sites where CO could be

Table 1
The energy barrier and reaction energy of forward reaction ($E_{a,f}$ and ΔE_f) and that of reverse reaction ($E_{a,r}$ and ΔE_r) on Pd_{ML}/SiC(111)-Si and on Pd_{ML}/SiC(111)-C terminal.

Surface	Elementary reaction	$E_{a,f}$ (kJ•mol^{-1})	ΔE_f (kJ•mol^{-1})	$E_{a,r}$ (kJ•mol^{-1})	ΔE_r (kJ•mol^{-1})
Pd_{ML}/SiC(111)-Si terminal	$CO + OCH_3 \rightarrow COOCH_3$	1.4	−11.3	12.8	11.3
	$COOCH_3 + CO + OCH_3 \rightarrow 2COOCH_3$	52.3	37.9	14.4	−37.9
	$2COOCH_3 \rightarrow (COOCH_3)_2$	88.9	−123.0	211.9	123.0
	$COOCH_3 + CO \rightarrow OCCOOCH_3$	107.5	60.3	47.1	−60.3
	$OCCOOCH_3 + OCH_3 \rightarrow (COOCH_3)_2$	84.6	−113.8	198.4	113.8
	$COOCH_3 + CO + OCH_3 \rightarrow DMC + CO$	116.1	−148.2	264.3	148.2
Pd_{ML}/SiC(111)-C terminal	$CO + OCH_3 \rightarrow COOCH_3$	43.7	−4.3	48.0	4.3
	$COOCH_3 + CO + OCH_3 \rightarrow 2COOCH_3$	68.3	3.6	64.7	−3.6
	$2COOCH_3 \rightarrow (COOCH_3)_2$	52.7	−120.6	173.3	120.6
	$COOCH_3 + CO \rightarrow OCCOOCH_3$	85.6	5.1	80.5	−5.1
	$OCCOOCH_3 + OCH_3 \rightarrow (COOCH_3)_2$	11.8	−184.3	196.1	184.3
	$COOCH_3 + CO + OCH_3 \rightarrow DMC + CO$	97.5	−102.1	266.0	102.1

adsorbed were Top, Hcp and Fcc sites, and its adsorption energies on the corresponding sites was −68.2, −104.8 and −102.0 kJ•mol^{-1}, respectively. OCH_3 could be adsorbed on four sites, and its adsorption energy was −117.2 on Top, −142.6 on Bridge, −182.2 on Hcp and −181.1 kJ•mol^{-1} on Fcc site. The sites that $COOCH_3$ and $OCCOOCH_3$ could adsorb were Top and Bridge sites, and their adsorption energies were −105.6 and −118.8 kJ•mol^{-1} as well as −94.1 and −146.1 kJ•mol^{-1}. The adsorption energies of DMO and DMC were −16.4 and −0.6 kJ•mol^{-1}, respectively. They were physical adsorption in the suspended state.

On the Pd_{ML}/SiC(111)-C terminal, the site for CO stable adsorption was the Top site, and its adsorption energy was −31.9 kJ•mol^{-1}. OCH_3 was only adsorbed on Hcp and Fcc sites with the adsorption energies of −108.0 and −154.9 kJ•mol^{-1}, respectively. The sites that $COOCH_3$ could adsorb were Top and Bridge sites, and its adsorption energies were −98.4 and −96.1 kJ•mol^{-1}, respectively. The site for $OCCOOCH_3$ stable adsorption was the Top site, and its adsorption energy was −71.7 kJ•mol^{-1}. DMO and DMC were physical adsorption, and their adsorption energies were −10.8 and 7.7 kJ•mol^{-1}, respectively.

Comparing the adsorption energies of these species on catalysts, it could be obtained that the adsorption energies of these species on Pd_{ML}/SiC(111)-Si terminal were stronger than those on Pd_{ML}/SiC(111)-C terminal. The differences in adsorption energies of these species would lead to the differences in catalytic performance of catalysts to a large extent.

3.2. Reaction mechanisms for DMO synthesis from CO and OCH_3

The initial reactant CH_3ONO in CO oxidative coupling to DMO was readily decomposed into the OCH_3 and NO [48,49]. Therefore, the dissociation of CH_3ONO would not be studied in this work, and the OCH_3 radical was thought as the initial species that induced DMO formation. In the light of the different coupling modes of C—C bond, there existed three reaction paths for CO oxidative coupling to DMO, which was $COOCH_3$-$COOCH_3$, $COOCH_3$-CO and CO—CO coupling path. For the OCCO intermediate could not survive stably on the Pd_{ML}/SiC(111)-Si and Pd_{ML}/SiC(111)-C terminal, the CO—CO coupling path was not considered. Only the two reaction paths, $COOCH_3$-$COOCH_3$ and $COOCH_3$-CO coupling path, were considered in this work, which was shown in Scheme 1. Previous studies [28,50,51] have demonstrated that CO in a weakly adsorbed way participated in DMO synthesis from CO and OCH_3, owing to the weak chemical adsorption making species easily activated. Therefore, the weakly adsorbed site was chosen as the reaction active site in the following study. The corresponding energy barrier and reaction energy of elementary reaction have been listed in Table 1.

3.2.1. Reaction mechanism for DMO formation on the Pd_{ml}/SiC(111)-Si terminal

As shown in Fig. 4, the initial reactants of OCH_3 and CO were firstly adsorbed at Top sites on the Pd_{ML}/SiC(111)-Si terminal, which induced the first elementary step of OCH_3 and CO mutual interaction to form $COOCH_3$ intermediate. The step was easy to happen, and the energy barrier which it needed to overcome was only 1.4 kJ•mol^{-1}, meanwhile it released the heat of 11.3 kJ•mol^{-1}. The distance of C1···O2 was shortened from 3.061 Å in the initial state to 2.172 Å in TS1. The produced $COOCH_3$ intermediate occupied on top site, then another reactants of OCH_3 and CO occupied on the Hcp and Top site, respectively, and the second $COOCH_3$ intermediate was generated through the interaction between OCH_3 and CO. The reaction energy barrier to be overcome in this step was 52.2 kJ•mol^{-1}, and the endothermic heat was 37.9 kJ•mol^{-1}. The distance of C3···O4 was diminished from 4.026 Å in the initial state to 1.897 Å in TS2. Ultimately, the DMO product was formed by mutual coupling of two $COOCH_3$ intermediates through TS3. The energy barrier and reaction energy were 88.9 and −123.0 kJ•mol^{-1}, respectively. The distance of C1···C3 in the initial state was shortened from 4.008 Å to 2.35 Å in TS3.

The first elementary step in Path2 was the same as that in Path1. On the foundation of $COOCH_3$ intermediate produced in the first step, another CO was adsorbed on the Hcp site. Then, $OCCOOCH_3$ intermediate was formed via $COOCH_3$ coupling with CO. The energy barrier to be overcome in this step was 107.5 kJ•mol$^{-1,}$ and the endothermic heat was 60.3 kJ•mol^{-1}. Meantime, the distance of C1···C3 was reduced to 2.020 Å in TS4 from 5.244 Å in the initial state. Finally, $OCCOOCH_3$ intermediate connected with OCH_3 to generate DMO through TS5. The activation energy and exothermic heat of the step were 84.6 and 113.8 kJ•mol^{-1}, respectively. The distance being 4.192 Å of C3···O4 in the initial state was shortened to 3.008 Å in TS5.

By comparing the activation energies of elementary steps in each reaction path, it was obtained that the rate control steps of Path 1 and Path 2 were $2COOCH_3 \rightarrow$ DMO and $COOCH_3 + CO \rightarrow OCCOOCH_3$, and their activation energies were 88.9 and 107.5 kJ•mol^{-1}, respectively. Obviously the optimum reaction path was Path1.

3.2.2. Reaction mechanism for DMO formation on the Pd_{ml}/SiC(111)-C terminal

On the Pd_{ML}/SiC(111)-C terminal, as shown in Fig. 5, the first elementary step in Path1 began with co-adsorption of OCH_3 and CO at Hcp and Top, respectively. Then, OCH_3 interacted with CO to form $COOCH_3$ intermediate. The energy barrier which the step needed to surmount was 43.7 kJ•mol^{-1}, and exothermic heat was 4.3 kJ•mol^{-1}. The C1···O2 distance was shortened from 3.484 Å in the initial state to 1.908 Å in TS1. Hereafter, another OCH_3 and CO occupied on the Hcp and Top site near the $COOCH_3$ intermediate, respectively. Immediately, OCH_3 and CO interacted with each other to form the second $COOCH_3$ intermediate. Its reaction energy barrier and endothermic heat were 68.3 and 3.6 kJ•mol^{-1}. The distance of C3···O4 was diminished from 4.986 Å in the initial state to 3.603 Å in TS2. Ultimately, the DMO product was formed via two $COOCH_3$ intermediates coupling with each other. The energy barrier to be conquered was 52.7 kJ•mol^{-1} and reaction energy was −120.6 kJ•mol^{-1}. The distance of C1···C3 in the initial state was shortened from 4.338 Å to 2.012 Å in TS3.

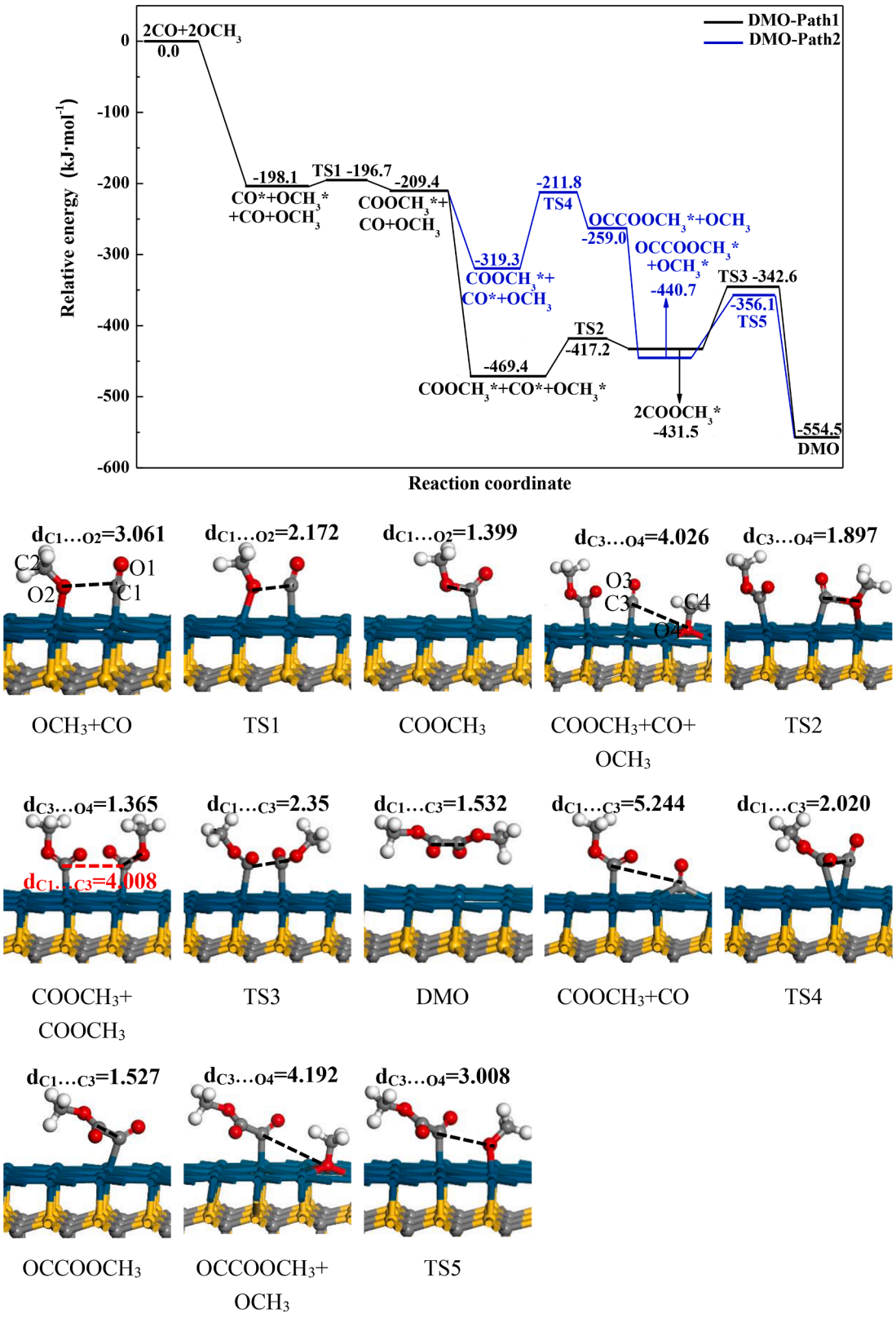

Fig. 4. The potential energy and structures profile for DMO synthesis from CO and OCH_3 on Pd_{ML}/SiC(111)-Si terminal.

In path 2, another CO was adsorbed at the top site, which was next to $COOCH_3$ intermediate produced in the first elementary step. Then, $COOCH_3$ was coupled with CO to form the $OCCOOCH_3$ intermediate. The energy barrier to be overcome in this step was 85.6 kJ•mol^{-1}, and the endothermic heat was 5.1 kJ•mol^{-1}. In TS4, the distance of C1···C3 was reduced from 3.587 Å in the initial state to 2.016 Å. Finally, the $OCCOOCH_3$ intermediate connected with OCH_3 to generate DMO by TS5. The activation energy and exothermic heat of the step were 11.8 and 184.3 kJ•mol^{-1}. The distance of C3…O4 in the initial state was shortened from 3.963 Å to 2.213 Å in TS5.

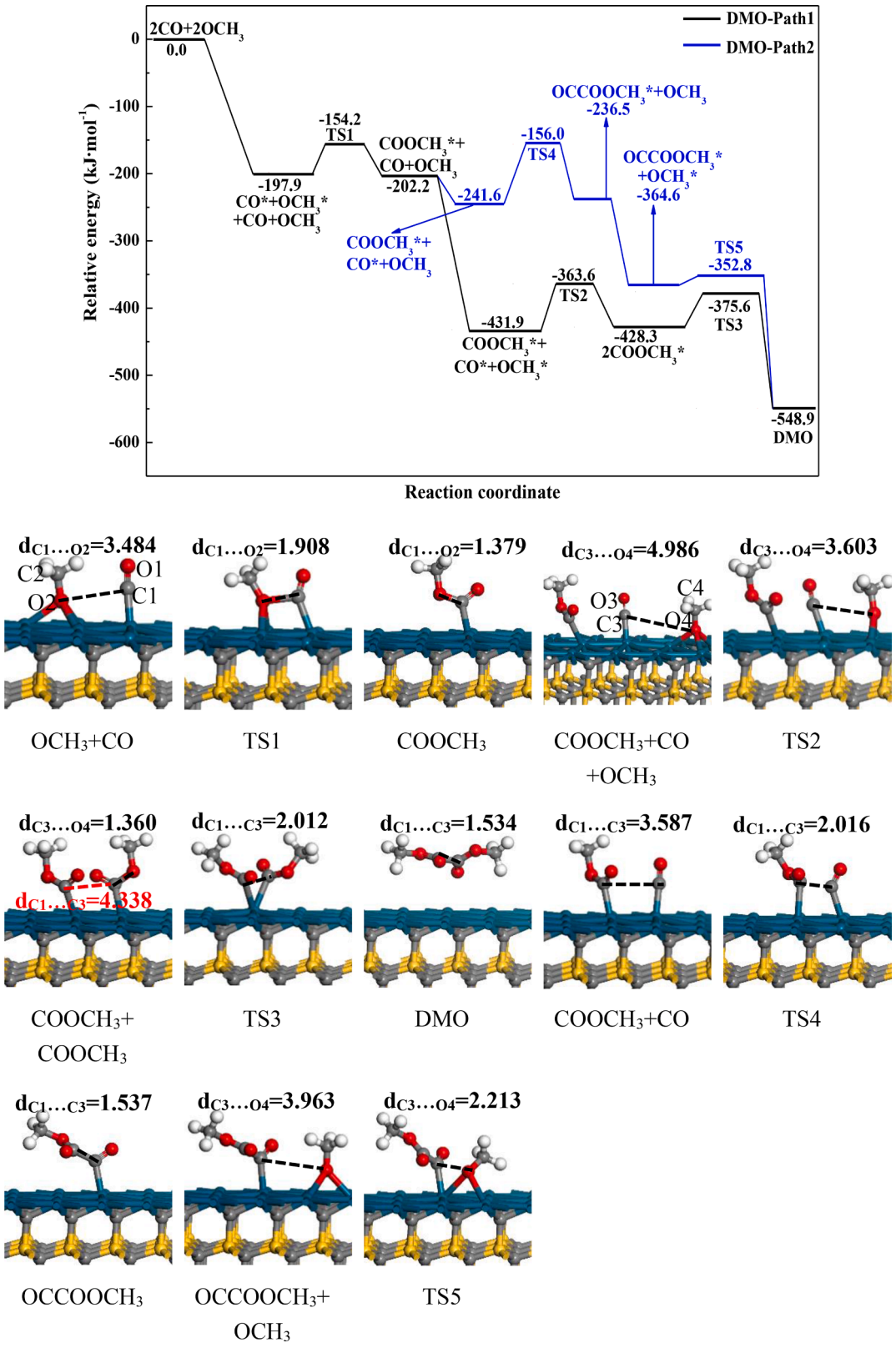

Fig. 5. The potential energy and structures profile for DMO synthesis from CO and OCH_3 on the Pd_{ML}/SiC(111)-C terminal.

In summary, the rate control steps of Path 1 and Path 2 were $COOCH_3 + CO + OCH_3 \rightarrow 2COOCH_3$ and $COOCH_3 + CO \rightarrow OCCOOCH_3$, and their activation energies were 68.3 and 85.6 kJ•mol^{-1}, respectively, indicating that Path1 was the optimum reaction path.

3.3. Comparison of side-product DMC and major-product DMO formation

In addition to research on the formation of major-product DMO, the formation of side-product DMC was also studied. DMC was formed by

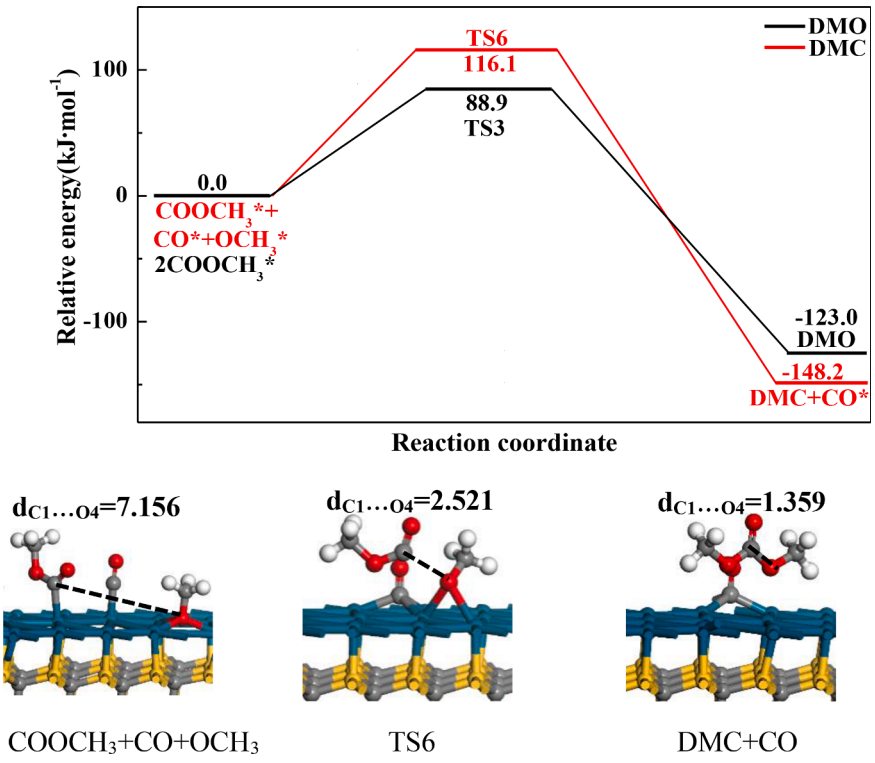

Fig. 6. The comparison of potential energy profile of side-product DMC and major-product DMO on the Pd_{ML}/SiC(111)-Si terminal.

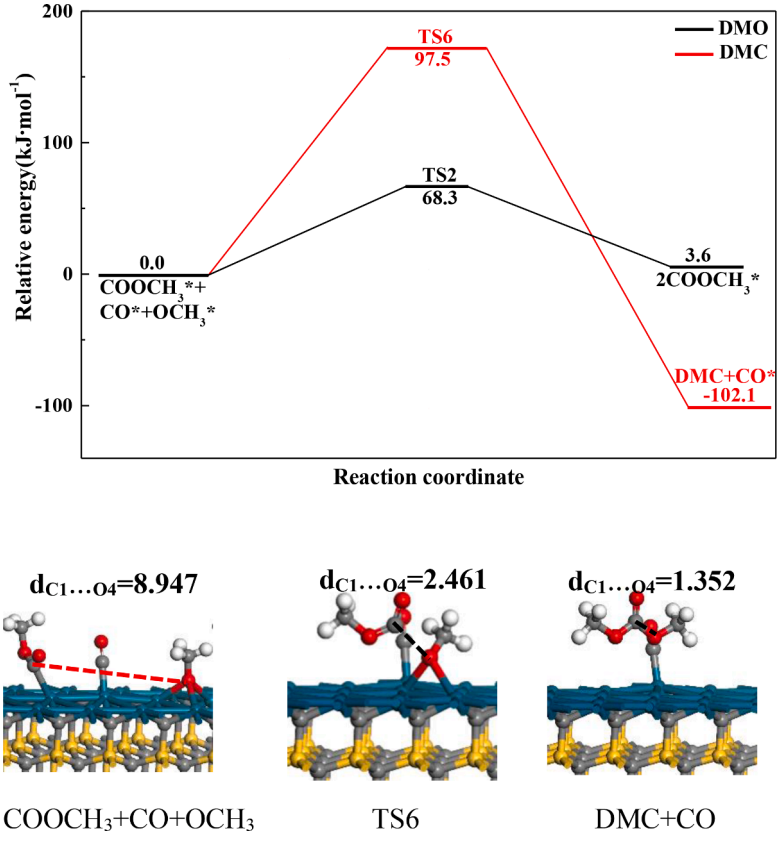

Fig. 7. The comparison of potential energy profile of side-product DMC and major-product DMO on the Pd_{ML}/SiC(111)-C terminal.

Table 2
The adsorption equilibrium constants and rate constant (k, s^{-1}) (T: 375–415 K).

		375 K	385 K	395 K	405 K	415 K
Pd_{ML}/SiC (111)-Si terminal	K_{CO}	2.94 × 10^4	1.65 × 10^4	9.53 × 10^3	5.65 × 10^3	3.44 × 10^3
	K_{OCH3}	2.99 × 10^{13}	1.79 × 10^{13}	7.03 × 10^{12}	2.90 × 10^{12}	1.25 × 10^{12}
	k_1	1.23 × 10^{12}	1.25 × 10^{12}	1.27 × 10^{12}	1.29 × 10^{12}	1.31 × 10^{12}
	k_2	9.43 × 10^5	1.47 × 10^6	2.25 × 10^6	3.37 × 10^6	4.94 × 10^6
	k_3	7.14 × 10^0	1.53 × 10^1	3.14 × 10^1	6.24 × 10^1	1.20 × 10^2
	k_4	1.80 × 10^{-2}	4.48 × 10^{-2}	1.07 × 10^{-1}	2.43 × 10^{-1}	5.32 × 10^{-1}
	k_5	1.40 × 10^1	2.88 × 10^1	5.70 × 10^1	1.09 × 10^2	2.03 × 10^2
	k_6	1.01 × 10^{-3}	2.70 × 10^{-3}	6.89 × 10^{-3}	1.68 × 10^{-2}	3.91 × 10^{-2}
	k_1^-	3.73 × 10^{11}	4.29 × 10^{11}	4.89 × 10^{11}	5.55 × 10^{11}	6.26 × 10^{11}
	k_2^-	3.81 × 10^{10}	4.40 × 10^{10}	5.04 × 10^{10}	5.74 × 10^{10}	6.50 × 10^{10}
	k_3^-	5.66 × 10^{-17}	3.46 × 10^{-16}	1.93 × 10^{-15}	9.90 × 10^{-15}	4.70 × 10^{-14}
	k_4^-	5.80 × 10^6	8.88 × 10^6	1.33 × 10^7	1.96 × 10^7	2.83 × 10^7
	k_5^-	3.46 × 10^{-16}	1.86 × 10^{-15}	9.23 × 10^{-15}	4.23 × 10^{-14}	1.80 × 10^{-13}
	k_6^-	3.69 × 10^{-24}	3.49 × 10^{-23}	2.94 × 10^{-22}	2.24 × 10^{-21}	1.55 × 10^{-20}
Pd_{ML}/SiC (111)-C terminal	K_{CO}	9.72 × 10^{-1}	7.41 × 10^{-1}	5.73 × 10^{-1}	4.49 × 10^{-1}	3.56 × 10^{-1}
	K_{OCH3}	1.95 × 10^{17}	8.75 × 10^{16}	2.55 × 10^{16}	7.90 × 10^{15}	2.59 × 10^{15}
	k_1	3.48 × 10^6	5.03 × 10^6	7.15 × 10^6	9.98 × 10^6	1.37 × 10^7
	k_2	8.12 × 10^3	1.46 × 10^4	2.55 × 10^4	4.34 × 10^4	7.20 × 10^4
	k_3	1.30 × 10^5	2.02 × 10^5	3.07 × 10^5	4.57 × 10^5	6.68 × 10^5
	k_4	1.28 × 10^0	2.63 × 10^0	5.20 × 10^0	9.95 × 10^0	1.84 × 10^1
	k_5	1.34 × 10^{10}	1.47 × 10^{10}	1.61 × 10^{10}	1.75 × 10^{10}	1.89 × 10^{10}
	k_6	1.17 × 10^{-10}	4.72 × 10^{-10}	1.77 × 10^{-9}	6.21 × 10^{-9}	2.05 × 10^{-8}
	k_1^-	2.89 × 10^5	4.41 × 10^5	6.60 × 10^5	9.68 × 10^5	1.39 × 10^6
	k_2^-	1.16 × 10^5	2.07 × 10^5	3.59 × 10^5	6.05 × 10^5	9.97 × 10^5
	k_3^-	1.52 × 10^{-13}	6.58 × 10^{-13}	2.65 × 10^{-12}	9.96 × 10^{-12}	3.52 × 10^{-11}
	k_4^-	3.87 × 10^1	7.82 × 10^1	1.53 × 10^2	2.89 × 10^2	5.29 × 10^2
	k_5^-	4.65 × 10^{-17}	2.43 × 10^{-16}	1.17 × 10^{-15}	5.20 × 10^{-15}	2.15 × 10^{-14}
	k_6^-	5.94 × 10^{-26}	5.67 × 10^{-25}	4.83 × 10^{-24}	3.71 × 10^{-23}	2.59 × 10^{-22}

the interaction of $COOCH_3$ intermediate with OCH_3, as presented in Figs. 6 and 7, where the influence of CO was taken into consideration, because CO was excessive in the actual reaction [50]. By the contrast of the activation barriers (88.9 vs 116.1, 68.3 vs 97.5) of the rate control steps in dominant paths about the DMO and DMC, we could know that it was more advantageous to generate DMO than DMC on Pd_{ML}/SiC (111)-Si and Pd_{ML}/SiC(111)-C terminal.

3.4. Micro-reaction kinetic model analysis

The micro-reaction kinetic model was the bridge between the micro and practical reaction. Hereupon, the work adopted micro-reaction kinetic model to study CO oxidative coupling to DMO on Pd_{ML}/SiC(111)-Si and Pd_{ML}/SiC(111)-C terminal under actual reaction conditions with

Table 3
The surface coverage of different species and formation rates (s^{-1}) of DMO and DMC (T: 375–415 K).

		375 K	385 K	395 K	405 K	415 K
Pd_{ML}/SiC (111)-Si terminal	θ_*	1.02 × 10^{-20}	2.48 × 10^{-20}	7.29 × 10^{-20}	2.03 × 10^{-19}	5.35 × 10^{-19}
	θ_{CO}	8.39 × 10^{-11}	1.14 × 10^{-10}	1.94 × 10^{-10}	3.21 × 10^{-10}	5.16 × 10^{-10}
	θ_{OCH3}	6.09 × 10^{-2}	8.85 × 10^{-2}	1.03 × 10^{-1}	1.18 × 10^{-1}	1.34 × 10^{-1}
	θ_{COOCH3}	9.38 × 10^{-1}	9.12 × 10^{-1}	8.99 × 10^{-1}	8.85 × 10^{-1}	8.68 × 10^{-1}
	$\theta_{OCCOOCH3}$	1.05 × 10^{-25}	4.43 × 10^{-25}	3.44 × 10^{-24}	2.40 × 10^{-23}	1.52 × 10^{-22}
	r_{DMO}	6.31 × 10^0	1.29 × 10^1	2.55 × 10^1	4.89 × 10^1	9.03 × 10^1
	r_{DMC}	5.81 × 10^{-5}	2.24 × 10^{-4}	6.35 × 10^{-4}	1.78 × 10^{-3}	4.55 × 10^{-3}
Pd_{ML}/SiC (111)-C terminal	θ_*	2.56 × 10^{-23}	5.71 × 10^{-23}	1.96 × 10^{-22}	6.33 × 10^{-22}	1.93 × 10^{-21}
	θ_{CO}	6.96 × 10^{-18}	1.19 × 10^{-17}	3.15 × 10^{-17}	7.96 × 10^{-17}	1.92 × 10^{-16}
	θ_{OCH3}	1.00 × 10^0	1.00 × 10^0	1.00 × 10^0	1.00 × 10^0	1.00 × 10^0
	θ_{COOCH3}	1.38 × 10^{-8}	1.77 × 10^{-8}	2.89 × 10^{-8}	4.80 × 10^{-8}	8.35 × 10^{-8}
	$\theta_{OCCOOCH3}$	6.58 × 10^{-49}	9.47 × 10^{-48}	3.05 × 10^{-46}	8.26 × 10^{-45}	1.91 × 10^{-43}
	r_{DMO}	2.47 × 10^{-11}	6.32 × 10^{-11}	2.56 × 10^{-10}	1.05 × 10^{-9}	4.66 × 10^{-9}
	r_{DMC}	1.62 × 10^{-18}	8.36 × 10^{-18}	5.11 × 10^{-17}	2.98 × 10^{-16}	1.72 × 10^{-15}
Pd(111) [28]	r_{DMO}	4.72 × 10^{-6}	1.29 × 10^{-5}	3.35 × 10^{-5}	5.31 × 10^{-5}	1.98 × 10^{-4}
	r_{DMC}	4.02 × 10^{-14}	2.45 × 10^{-13}	1.11 × 10^{-12}	4.02 × 10^{-12}	6.04 × 10^{-12}

pressures (P_{CO}: 280 kPa, P_{CH3ONO}: 200 kPa) and temperatures (T: 375−415 K) [16].

The adsorption process of the initial reactants (CO and OCH_3) was assumed to be equilibrium. The K of equilibrium constants and the k of rate constants could be obtained by formulas (7), (8), (9) and (10), respectively, which was presented in Table 2. In this model, we not only consider the positive reaction but also the reverse reaction. Each species coverage and the production rate of DMO and DMC were obtained by formulas (11)–(15) and (16),(17), respectively, and the results were listed in Table 3.

$$K = \exp\left[-\left(\Delta E_{ads} - T\left(S_{adsorbate} - S_{gas}\right)\right)/RT\right] \tag{7}$$

$$S = R\sum_{i=1}^{3N}\left[-\ln\left(1-\exp\left(-\frac{h\nu_i}{k_B T}\right)\right) + \frac{h\nu_i}{k_B T}\frac{\exp\left(-\frac{h\nu_i}{k_B T}\right)}{1-\exp\left(-\frac{h\nu_i}{k_B T}\right)}\right] \tag{8}$$

$$k = \frac{k_B T}{h}\frac{\prod_{i=1}^{3N}\left[1-\exp\left(-\frac{h\nu_i^{IS}}{k_B T}\right)\right]}{\prod_{i=1}^{3N-1}\left[1-\exp\left(-\frac{h\nu_i^{TS}}{k_B T}\right)\right]}\exp\left(\frac{-Ea,f}{RT}\right) \tag{9}$$

$$k^- = \frac{k_B T}{h}\frac{\prod_{i=1}^{3N}\left[1-\exp\left(-\frac{h\nu_i^{FS}}{k_B T}\right)\right]}{\prod_{i=1}^{3N-1}\left[1-\exp\left(-\frac{h\nu_i^{TS}}{k_B T}\right)\right]}\exp\left(\frac{-Ea,r}{RT}\right) \tag{10}$$

$$\theta_{CO} = P_{CO}K_{CO}\theta^* \tag{11}$$

$$\theta_{OCH_3} = P_{OCH_3}K_{OCH_3}\theta^* \tag{12}$$

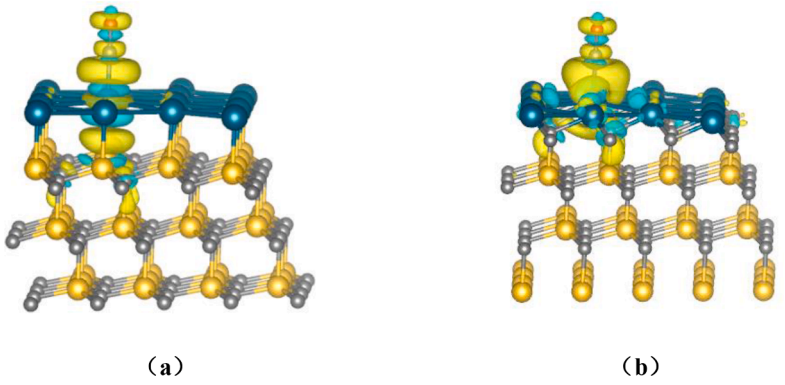

Fig. 8. The differential charge density of CO adsorbed on top site over Pd_{ML}/SiC(111)-Si **(a)** and Pd_{ML}/SiC(111)-C terminal **(b).** (Blue shaded regions: charge gain; yellow shaded regions, charge loss).

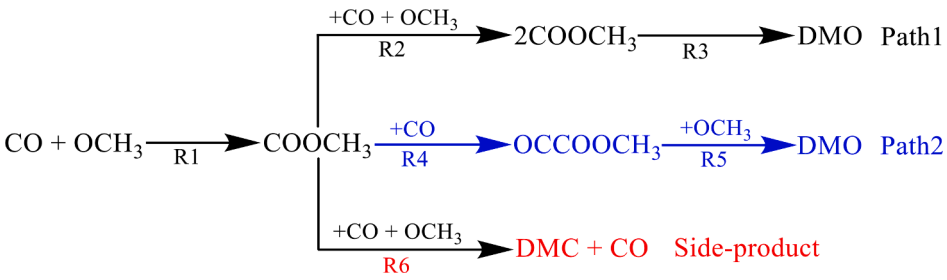

Scheme 1. Proposed reaction paths [50] for DMO synthesis from CO and OCH_3.

$$\theta_{COOCH_3}: \frac{d\theta_{COOCH_3}}{dt} = k_1\theta_{OCH_3}\theta_{CO} - k_1^-\theta_{COOCH_3}\theta^* + k_2\theta_{OCH_3}\theta_{CO} - k_2^-\theta_{COOCH_3}\theta^* + k_3\theta_{COOCH_3}^2 - k_4\theta_{COOCH_3}\theta_{CO} + k_4^-\theta_{OCCOOCH_3}\theta^* - k_6\theta_{COOCH_3}\theta_{OCH_3} = 0 \quad (13)$$

$$\theta_{OCCOOCH_3}: \frac{d\theta_{OCCOOCH_3}}{dt} = k_4\theta_{COOCH_3}\theta_{CO} - k_4^-\theta_{OCCOOCH_3}\theta^* - k_5\theta_{OCCOOCH3}\theta_{OCH_3} = 0 \quad (14)$$

$$\theta_{CO} + \theta_{OCH_3} + \theta_{COOCH_3} + \theta_{OCCOOCH_3} + \theta^* = 1 \quad (15)$$

$$r_{DMO} = k_3\theta_{COOCH_3}^2 + k_5\theta_{OCCOOCH_3}\theta_{OCH_3} \quad (16)$$

$$r_{DMC} = k_6\theta_{COOCH_3}\theta_{OCH_3} \quad (17)$$

In the above formulas, k_B refers to Boltzmann constant; ν_i^{IS} *and* ν_i^{TS} refer to real frequencies of initial and transition state, respectively; ΔE_{ads} and $S_{adsorbate}$ refer to the adsorption energies and entropies of CO and OCH_3 of the initial reactants, respectively; S_{gas} refers to the gas phase entropy.

Previous studies indicated the catalytic performance of Pd(111) surface was close to that of industrial catalysts (Pd/a-Al_2O_3) toward CO oxidative coupling to DMO [16]. Therefore, the results of micro-reaction kinetic model analysis about Pd_{ML}/SiC(111)-Si and Pd_{ML}/SiC(111)-C terminal were compared with that of Pd(111), which hope to obtain better silicon carbide-supported Pd catalysts. The corresponding comparison results were as indicated in Table 3, it was obtained that the DMO formation rate was in regular succession of Pd_{ML}/SiC(111)-Si terminal > Pd(111) > Pd_{ML}/SiC(111)-C terminal. The DMO formation rate was far better than that of DMC on these catalysts. In conclusion, it was found that the Pd_{ML}/SiC(111)-Si terminal possessed not only excellent activity but also outstanding selectivity for DMO generation among these catalysts. The similar micro-reaction kinetic model analysis has been successfully adopted to evaluate the catalytic performance of catalysts toward DMO synthesis from CO and OCH_3 [28,52].

3.5. Analysis of factors affecting catalytic activity for DMO synthesis

The catalyst usually facilitates chemical reactions through electronic interactions between it with guest molecules. In this work, the differential charge density and bader charge analysis were adopted to calculated charge transfer of Pd monolayer about the example of CO adsorbed on top site. The differential charge density plot in Fig. 8 indicated that on the Pd_{ML}/SiC(111)-Si terminal, the electron transferred from Si terminal to Pd monolayer, then from Pd monolayer to CO; on the Pd_{ML}/SiC(111)-C teminal, the electron transferred from Pd monolayer bidirectionally to C terminal and adsorbent CO. The Bader charge analysis further obtained that Pd monolayer got the charge of 0.41 *e* on the Pd_{ML}/SiC(111)-Si terminal, but lost the charge of 0.25 *e* on the Pd_{ML}/SiC(111)-C teminal.

This electronic interaction was mainly reflected in the adsorption energy of guest molecules on the catalyst [53]. Compared with that on Pd_{ML}/SiC(111)-C terminal, the adsorption energies of reactants (CO, OCH_3) and key intermediates ($COOCH_3$, $OCCOOCH_3$) were moderate strong chemical adsorption on Pd_{ML}/SiC(111)-Si terminal, which ensured them could be not only adsorbed stably but also easily activated. The difference in adsorption energy further resulted in different rate control steps of the optimal pathway, which was $2COOCH_3$ →DMO and $COOCH_3$ + (CO + OCH_3) → $2COOCH_3$ on the Pd_{ML}/SiC(111)-Si and Pd_{ML}/SiC(111)-C terminal, respectively. It led to the coverage of key intermediate $COOCH_3$ determining the yield of DMO on the Pd_{ML}/SiC(111)-Si terminal was much greater than that on the Pd_{ML}/SiC(111)-C terminal, further resulted in that the DMO formation rate on the Pd_{ML}/SiC(111)-Si terminal was higher than that on the Pd_{ML}/SiC(111)-C terminal. The above factors were presumed to be the main reasons about that the catalytic performance of Pd_{ML}/SiC(111)-Si terminal was favorable than that of Pd_{ML}/SiC(111)-C terminal.

4. Conclusions

Using DFT calculations combined with the micro-reaction kinetic model analysis, we have investigated the effects of different exposed terminals of SiC substrate toward Pd catalytic CO oxidation to DMO. It could be concluded the $COOCH_3$-$COOCH_3$ coupling path was the optimum to generate DMO on the Pd_{ML}/SiC(111)-Si terminal, which had no difference with that on Pd_{ML}/SiC(111)-C terminal. However, the rate control step of the optimum path was $2COOCH_3$ → DMO on the Pd_{ML}/SiC(111)-Si terminal, which was different with that on the Pd_{ML}/SiC(111)-C terminal. Moreover, it was obtained that the Pd_{ML}/SiC(111)-Si terminal exhibited excellent catalytic performance than Pd_{ML}/SiC(111)-C terminal, which was mainly resulted from the difference of electrons transfer direction of Pd monolayer causing the difference in adsorption energies of reactants and key intermediates as well as rate control steps in the optimum path on two catalysts. This finding can provide the theoretical insights for designing of supported Pd-based catalyst for heterogeneous catalytic reaction.

CRediT authorship contribution statement

Bingying Han: Conceptualization, Data curation, Formal analysis, Validation, Writing – original draft. **Mengjie Dong:** Data curation, Formal analysis. **Riguang Zhang:** Supervision, Funding acquisition. **Lixia Ling:** Conceptualization, Funding acquisition, Investigation, Methodology, Project administration, Resources, Software, Validation, Writing – review & editing. **Maohong Fan:** . **Ping Liu:** . **Baojun Wang:** Investigation, Methodology, Software, Supervision, Writing – review & editing, Funding acquisition.

Declaration of Competing Interest

The authors declare that they have no known competing financial interests or personal relationships that could have appeared to influence the work reported in this paper.

Acknowledgments

This work was financially supported by the National Natural Science Foundation of China (Grant Nos. 21576178 and 21476155), the Key Projects of National Natural Science Foundation of China (21736007), the Foundation of State Key Laboratory of Coal Conversion (No. J18–19–602) and the Research Project Supported by Shanxi Scholarship Council of China (No. 2016–030).

References

[1] Q. Yi, W.Y. Li, J. Feng, K.C. Xie, Carbon cycle in advanced coal chemical engineering, Chem. Soc. Rev. 44 (2015) 5409–5445.
[2] Q.Q. Chen, M. Lv, Y. Gu, X.Y. Yang, Z.Y. Tang, Y.H. Sun, M.H. Jiang, Hybrid energy system for a coal-based chemical industry, Joule 2 (2018) 607–620.
[3] H.J. Pan, S.G. Shen, T.J. Li, X. Wen, X.P. Ma, Z.J. Zhou, J. Li, C. Wang, B. Wu, S. Q. Jing, A simple strategy for the preparation of chlorine functionalized coal-based solid acid with rich carboxyl to improve the activity for hydrolysis of cellulose, Mol. Catal. 492 (2020), 111015-1-8.
[4] F. Zhang, Y.L. Zhang, Y. Liu, K.A.M. Gasem, J.Y. Chen, F.K. Chiang, Y.G. Wang, M. H. Fan, Synthesis of Cu/Zn/Al/Mg catalysts on methanol production by different precipitation methods, Mol. Catal. 441 (2017) 190–198.
[5] X.Y. Xu, Y. Liu, F. Zhang, W. Di, Y.L. Zhang, Clean coal technologies in China based on methanol platform, Catal. Today 298 (2017) 61–68.
[6] L.Y. Rong, Z.N. Xu, J. Sun, G.C. Guo, New methyl formate synthesis method: coal to methyl formate, J. Energy Chem. 27 (2018) 238–242.
[7] H.H. Schobert, C. Song, Chemicals and materials from coal in the 21st century, Fuel 81 (2002) 15–32.
[8] J.Y. Li, H.X. Liu, W.Y. Gou, M.K. Zhang, Z.M. Xia, S. Zhang, C.R. Chang, Y.Y. Ma, Y. Q. Qu, Ethylene-glycol ligand environment facilitates highly efficient hydrogen evolution of Pt/CoP through proton concentration and hydrogen spillover, Energy Environ. Sci. 12 (2019) 2298–2304.
[9] Y.Q. Zou, N.V. Wolff, A. Anaby, Y.J. Xie, D. Milstein, Ethylene glycol as an efficient and reversible liquid-organic hydrogen carrier, Nat. Catal. 2 (2019) 415–422.
[10] Y.F. Zhu, X. Kong, H.Y. Zheng, Y.L. Zhu, Strong metal-oxide interactions induce bifunctional and structural effects for Cu catalysts, Mol. Catal. 458 (2018) 73–82.
[11] J. Ding, Y.T. Liu, J. Zhang, M. Dong, Y.X. Wang, W.X. He, X.X. Han, K.F. Liu, Z. Jiang, J.G. Chen, Synergism from interfaces between Cu and crystalline ZrO_2 nanosheets fabricated by acetic complex method for oxalates hydrogenation, Mol. Catal. 438 (2017) 93–102.
[12] J.J. Chen, Y. Qian, S.Y. Yang, Conceptual design and techno-economic analysis of a coal to methanol and ethylene glycol cogeneration process with low carbon emission and high efficiency, ACS Sustain. Chem. Eng. 8 (2020) 5229–5239.
[13] H.R. Yue, Y.J. Zhao, X.B. Ma, J.L. Gong, Ethylene glycol: properties, synthesis, and applications, Chem. Soc. Rev. 41 (2012) 4218–4244.
[14] Z.Q. Wang, J. Sun, Z.N. Xu, G.C. Guo, CO direct esterification to dimethyl oxalate and dimethyl carbonate: the key functional motifs for catalytic selectivity, Nanoscale 12 (2020) 20131–20140.
[15] Y.Q. Qu, Y. Wang, J.W. Li, Q.X. Xu, X. Liang, A.R. Jiang, Insights into the Pd nanocatalysts directed by morphology effect for CO and methyl nitrite coupling to dimethyl oxalate, Mol. Catal. 490 (2020), 110949-1-8.
[16] Z.N. Xu, J. Sun, C.S. Lin, X.M. Jiang, Q.S. Chen, S.Y. Peng, M.S. Wang, G.C. Guo, High-performance and long-lived Pd nanocatalyst directed by shape effect for CO oxidative coupling to dimethyl oxalate, ACS Catal. 3 (2013) 118–122.
[17] S.Y. Peng, Z.N. Xu, Q.S. Chen, Y.M. Chen, J. Sun, Z.Q. Wang, M.S. Wang, G.C. Guo, An ultra-low Pd loading nanocatalyst with high activity and stability for CO oxidative coupling to dimethyl oxalate, Chem. Commun. 49 (2013) 5718–5720.
[18] Y.F. Liu, B. Tymowski, F. Vigneron, I. Florea, O. Ersen, C. Meny, P. Nguyen, C. Pham, F. Luck, C.P. Huu, Titania-decorated silicon carbide-containing cobalt catalyst for fischer-tropsch synthesis, ACS Catal. 3 (2013) 393–404.
[19] H. Wang, R. Schmack, B. Paul, M. Albrecht, S. Sokolov, S. Rümmler, E. V. Kondratenko, R. Kraehnert, Porous silicon carbide as a support for Mn/Na/W/SiC catalyst in the oxidative coupling of methane, Appl. Catal. A Gen. 537 (2017) 33–39.
[20] Z.J. Yu, H.L. Tian, K. Sun, Y.W. Shao, L.J. Zhang, S. Zhang, P.G. Duan, Q. Liu, S. L. Niu, D.H. Dong, X. Hu, Impacts of externally added Brønsted and Lewis acid on conversion of furfural to cyclopentanone over Ni/SiC catalyst, Mol. Catal. 496 (2020), 111187-1-9.
[21] M. Afsharpour, A.R. Amraee, Synthesis of bio-inspired N-doped SiC and investigation of its synergetic effects on Mo catalysts in oxidative desulfurization reaction, Mol. Catal. 436 (2017) 285–293.
[22] Z.L. Guo, Y.F. Liu, Y. Liu, W. Chu, Promising SiC support for Pd catalyst in selective hydrogenation of acetylene to ethylene, Appl. Surf. Sci. 442 (2018) 736–741.
[23] X.N. Guo, G.J. Zhi, X.Y. Yan, G.Q. Jin, X.Y. Guo, P. Brault, Methane combustion over Pd/ZrO_2/SiC, Pd/CeO_2/SiC, and Pd/$Zr_{0.5}Ce_{0.5}O_2$/SiC catalysts, Catal. Commun. 12 (2011) 870–874.
[24] Y. Zhang, G. Gajjala, T. Hofmann, L. Weinhardt, M. Bär, C. Heske, M. Seelmann-Eggebert, P. Meisen, X-ray photoelectron spectroscopy study of the chemical interaction at the Pd/SiC interface, J. Appl. Phys. 108 (2010), 093702-1-6.
[25] M. Preuss, F. Bechstedt, W.G. Schmidt, J. Sochos, B. Schröter, W. Richter, Clean and pyrrole-functionalized Si- and C-terminated SiC surfaces: first-principles calculations of geometry and energetics compared with LEED and XPS, Phys. Rev. B 74 (2006), 235406-1-8.
[26] X.Q. Gong, Z.P. Liu, R. Raval, P. Hu, A systematic study of CO oxidation on metals and metal oxides: density functional theory calculations, J. Am. Chem. Soc. 126 (2004) 8–9.
[27] J.K. Nørskov, T. Bligaard, J. Rossmeisl, C.H. Christensen, Towards the computational design of solid catalysts, Nat. Chem. 1 (2009) 37–46.
[28] B.Y. Han, X. Feng, L.X. Ling, M.H. Fan, P. Liu, R.G. Zhang, B.J. Wang, CO oxidative coupling to dimethyl oxalate over Pd-Me (Me = Cu, Al) catalysts: a combined DFT and kinetic study, Phys. Chem. Chem. Phys. 20 (2018) 7317–7332.
[29] M.H. Butt, S.H.M. Zaidi, N.A. Khan, K. Ayub, M. Yar, M.A. Hashmi, M.A. Yawer, M. A. Zia, Cu-doped phosphorene as highly efficient single atom catalyst for CO oxidation: a DFT study, Mol. Catal. 509 (2021), 111630-1-9.
[30] Y.Y. Guo, Y.C. Dong, Z.G. Lei, Z.X. Liu, J.Q. Zhu, High-performance Pd-N (N = Ga or Ag) bimetallic monolithic catalyst for the hydrogenation of 2-ethylanthraquinone: experimental and DFT studies, Mol. Catal. 509 (2021), 111604-1-12.
[31] Y.B. He, J.F. Jia, H.S. Wu, First-principles investigation of the molecular adsorption and dissociation of hydrazine on Ni-Fe alloy surfaces, J. Phys. Chem. C 119 (2015) 8763–8774.
[32] J.F. Wang, W.S. Hao, L.J. Ma, J.F. Jia, H.S. Wu, The effect of interstitial boron on the mechanisms of acetylene hydrogenation catalyzed by Pd6: a DFT study, Comput. Theor. Chem. 1170 (2019), 112636-1-9.
[33] Z.P. Liu, P. Hu, General rules for predicting where a catalytic reaction should occur on metal surfaces: a density functional theory study of C-H and C-O bond breaking/making on flat, stepped, and kinked metal surfaces, J. Am. Chem. Soc. 125 (2003) 1958–1967.
[34] L.L. Ma, C.Q. Lv, G.C. Wang, A DFT study and micro-kinetic analysis of acetylene selective hydrogenation on Pd-doped Cu(111) surfaces, Appl. Surf. Sci. 410 (2017) 154–165.
[35] M.H. Hansen, J.K. Nørskov, T. Bligaard, First principles micro-kinetic model of catalytic non-oxidative dehydrogenation of ethane over close-packed metallic facets, J. Catal. 374 (2019) 161–170.
[36] B.A. Rohr, A.R. Singh, J.A. Gauthier, M.J. Statt, J.K. Nørskov, Micro-kinetic model of electrochemical carbon dioxide reduction over platinum in non-aqueous solvents, Phys. Chem. Chem. Phys. 22 (2020) 9040–9045.
[37] B.Y. Han, L.X. Ling, M.H. Fan, P. Liu, R.G. Zhang, B.J. Wang, Dimethyl oxalate synthesis via CO oxidation on Pd-doped Ag(111) surface: a theoretic study, Mol. Catal. 484 (2020), 110731-1-12.
[38] Y.J. Zhang, X.R. Shi, C.Y. Sun, S.M. Huang, Z.C. Duan, P. Ma, J.G. Wang, CO oxidation on Ni-based single-atom alloys surfaces, Mol. Catal. 495 (2020), 111154-1-10.

[39] J. Hafner, Materials simulations using VASP-a quantum perspective to materials science, Comput. Phys. Commun. 177 (2007) 6–13.
[40] G.Y. Sun, J. Kürti, P. Rajczy, M. Kertesz, J. Hafner, G. Kresse, Performance of the Vienna ab initio simulation package (VASP) in chemical applications, J. Mol. Struct. Theochem. 624 (2003) 37–45.
[41] I.H. Lee, R.M. Martin, Applications of the generalized-gradient approximation to atoms, clusters, and solids, Phys. Rev. B 56 (1997) 7197–7205.
[42] G. Kresse, D. Joubert, From ultrasoft pseudopotentials to the projector augmented-wave method, Phys. Rev. B 59 (1999) 1758–1775.
[43] P.E. Blöchl, O. Jepsen, O.K. Andersen, Improved tetrahedron method for Brillouin-zone integrations, Phys. Rev. B 49 (1994) 16223–16233.
[44] D. Sheppard, P.H. Xiao, W. Chemelewski, D.D. Johnson, G. Henkelman, A generalized solid-state nudged elastic band method, J. Chem. Phys. 136 (2012), 074103-1-8.
[45] P. Maragakis, S.A. Andreev, Y. Brumer, D.R. Reichman, E. Kaxiras, Adaptive nudged elastic band approach for transition state calculation, J. Chem. Phys. 117 (2002) 4651–4658.
[46] A. Heyden, A.T. Bell, F.J. Keil, Efficient methods for finding transition states in chemical reactions: comparison of improved dimer method and partitioned rational function optimization method, J. Chem. Phys. 123 (2005), 224101-1-14.
[47] G. Henkelman, H. Jónsson, A dimer method for finding saddle points on high dimensional potential surfaces using only first derivatives, J. Chem. Phys. 111 (1999) 7010–7022.
[48] C. Fan, M. Luo, W.D. Xiao, Reaction mechanism of methyl nitrite dissociation during CO catalytic coupling to dimethyl oxalate: a density functional theory study, Chin. J. Chem. Eng. 24 (2016) 132–139.
[49] J.W. Peck, D.I. Mahon, D.E. Beck, B. Bansenaur, B.K. Koe, TPD, HREELS and UPS study of the adsorption and reaction of methyl nitrite (CH_3ONO) on Pt(111), Surf. Sci. 410 (1998) 214–227.
[50] Q.H. Li, Z.F. Zhou, R.P. Chen, B.Z. Sun, L.Y. Qiao, Y.G. Yao, K.C. Wu, Insights into the reaction mechanism of CO oxidative coupling to dimethyl oxalate over palladium: a combined DFT and IR study, Phys. Chem. Chem. Phys. 17 (2015) 9126–9134.
[51] F.D. Meng, G.H. Xu, R.Q. Guo, H.F. Yan, M.Q. Chen, Kinetic study of carbon monoxide coupling reaction over supported palladium catalyst, Chem. Eng. Process. 43 (2004) 785–790.
[52] B.Y. Han, L.X. Ling, M.H. Fan, P. Liu, B.J. Wang, R.G. Zhang, A DFT study and microkinetic analysis of CO oxidation to dimethyl oxalate over Pd stripe and Pd single atom-doped Cu(111) surfaces, Appl. Surf. Sci. 479 (2019) 1057–1067.
[53] Y. Gamboa, A.A. Jalila, S. Triwahyonoc, A.A. Abdulrasheed, Recent advances and future prospect in catalysts for oxidative coupling of methane to ethylene: a review, J. Ind. Eng. Chem. 59 (2018) 218–229.